Fluorescence Lifetime and Blinking of Individual Semiconductor Nanocrystals on Graphene

Benoit Rogez, Heejun Yang, Eric Le Moal, Sandrine Leveque-Fort, Elizabeth Boer-Duchemin, Fei Yao, Young-Hee Lee, Yang Zhang, K. David Wegner, Niko Hildebrandt, et al.

Optical and electrical excitation of hybrid guided modes in an organic nanofiber-gold film system

Benoît Rogez,[†,¶] Rebecca Horeis,[‡] Eric Le Moal,[*,†] Jens Christoffers,[‡] Katharina Al-Shamery,[‡] Gérald Dujardin,[†] and Elizabeth Boer-Duchemin[†]

Institut des Sciences Moléculaires d´Orsay, CNRS - Université Paris-Sud (UMR 8214), Orsay, France, and Institut für Chemie & Center of Interface Science, Universität Oldenburg, 26129 Oldenburg, Germany

E-mail: eric.le-moal@u-psud.fr

Phone: +33 1 69 15 66 97. Fax: +33 1 69 15 67 77

[*]To whom correspondence should be addressed

[†]ISMO, Orsay, France

[‡]University of Oldenburg, Germany

[¶]Now at: Ludwig-Maximilians-Universität München, Department of Cellular Physiology, München, Germany.

Abstract

We report on the optical and electrical excitation of the modes of a "hybrid" waveguide consisting of a single organic nanofiber on a thin gold film. In the first set of experiments, *light* is used to excite the photoluminescence of an organic nanofiber on a thin gold film and the resulting emission is analyzed using Fourier-space leakage radiation microscopy. Two guided modes and the dispersion relations of this hybrid waveguide are thus determined. From numerical calculations, both a fundamental and excited mode of mixed photonic-plasmonic character are identified. In a second experiment, a local, *electrical* nanosource of surface plasmon polaritons (SPPs) is coupled to the hybrid waveguide. The SPP nanosource consists of the inelastic electron tunnel current between the tip of a scanning tunneling microscope (STM) and the gold film. We show that the electrically excited SPPs couple to the fundamental mode and that the coupling efficiency is highest when the SPP nanosource is aligned with the nanofiber axis. Moreover, the electrically excited SPPs strongly scatter into out-of-plane light at the nanofiber end. This light from scattered SPPs measured in the substrate is phase shifted by about π with respect to the direct light emission from beneath the STM tip. These experiments lead to a better understanding of the processes that must be optimized in order to exploit such hybrid waveguide structures.

Keywords

organic nanofiber, surface plasmon, photonic waveguide, hybrid nanostructure, leakage radiation microscopy, scanning tunneling microscopy

Introduction

Confining and guiding electromagnetic waves on a deep subwavelength scale is a long-sought-after goal and an essential step towards the integration of optics with nanoelectronics on a chip.[1,2] In particular, "hybrid" waveguides with mixed photonic-plasmonic guided modes

have been developed for the low-loss transport of light along quasi-1D structures.[3,4] Numerous designs of ultracompact optical components and circuitry based on dieletric-loaded surface plasmon polariton waveguides (DLSPPWs) made by top-down fabrication techniques have been reported.[5–9] Such waveguides consist of dielectric stripes atop a flat metallic surface and have generated much attention since the top-down fabrication process provides great flexibility in the design of the dielectric stripes. Though less studied, bottom-up fabrication based on chemically grown dielectric nanowires has also been touted recently for its simplicity and the availability of a broad variety of materials.[10–12] In particular, crystalline organic nanofibers are of specific interest for their high quantum yield photoluminescence,[13,14] which may be used in the development of integrated active waveguides with loss compensation or ultracompact organic lasers.[15–17] Organic nanofibers have been deposited on gold and silver films to form hybrid waveguides with low-loss guided modes of mixed photonic and plasmonic character,[18–20] and their dispersion relations have been measured.[21] However, until now, the optical behavior of such hybrid waveguides has only been studied using far-field photonic excitation; yet a local, electrical excitation source is to be favored in the context of integrated optical waveguides.[22]

In this article, we report on the use of a local, electrical nanosource of surface plasmon polaritons (SPPs) for the excitation of the hybrid guided modes of an organic nanofiber on a gold film. First of all, we *optically* excite the photoluminescence of a single nanofiber on a gold film which in turn couples to the guided modes of this hybrid system. The dispersion relations of the guided modes may then be determined by monitoring the resulting emission in Fourier space. Two different guided modes are identified from finite-difference time-domain (FDTD) calculations. Secondly, we use a local, *electrical* nanosource of SPPs on the gold film based on the inelastic tunneling of electrons from the tip of a scanning tunneling microscope (STM).[23] The coupling of the resulting circular SPP wave to the guided modes of a nearby nanofiber is studied by analyzing the leakage radiation in the real and Fourier spaces as a function of the relative lateral position of the STM tip with respect to the nanofiber end.

Finally, we investigate the properties of SPP scattering into light by a nanofiber.

Results and discussion

Sample properties and preparation

Organic nanofibers are synthesized by template growth in a nanoporous alumina matrix with pore sizes of 300 nm on average. This is a very versatile method for growing nanofibers from a variety of organic molecules (see details in the methods section).

The choice of diethyl 2,5-bis(phenylamino) terephthalate (see molecular structure in Fig. 1a) is motivated by the photoluminescence properties of the molecule which are used in this study to retrieve the dispersion relations of the nanofiber guided modes. Figure 1a shows the absorption and fluorescence spectra of the molecule in a CH_2Cl_2 (dichloromethane) solution (solid lines), as well as the fluorescence spectra of the molecule in the solid state (dotted line: powder, dashed line: nanofibers). The optical absorption and emission bands of the molecule lie almost entirely outside and inside the spectral domain of SPPs existing on an air|gold interface, respectively. Thus, the photoluminescence of the organic nanofibers may be excited without coupling the incident light to SPPs on the gold film; as a result, only the nanofiber emission couples to SPPs.

After the synthesis and dispersion of the nanofibers in solution, a droplet of the solution is deposited on a substrate (either a glass coverslip or a 50 nm-thick gold film thermally evaporated on glass). Scanning electron micrographs of the resulting fibers may be seen in parts b,c of Fig. 1. Figure 1d,e shows a topographic image of a single nanofiber on the gold film, measured by atomic force microscopy (AFM), and a height profile measured along a cross section of the nanofiber. In general, we observe nanofibers with homogeneous diameters of 300 nm and lengths ranging from 1 μm to 15 μm.

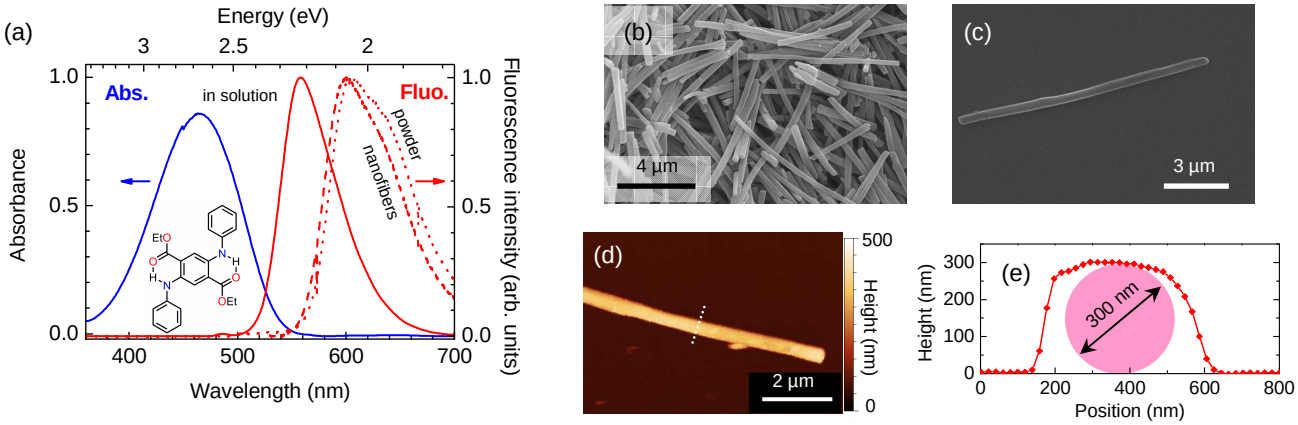

Figure 1: Characterization of the organic molecule and nanofibers. (a) Optical absorption and fluorescence spectra of diethyl 2,5-bis(phenylamino)terephthalate ($C_{24}H_{24}N_2O_4$, molecular structure in inset) diluted in dichloromethane (CH_2Cl_2) at a concentration of 0.1 mg/ml (solid lines); fluorescence spectra of the molecule in powdered form (dotted line) and as nanofibers (dashed line). All fluorescence spectra are measured using laser excitation at 488 nm. (b,c) Scanning electron micrographs of (b) a powder of well-separated organic nanofibers obtained after purification of the synthesis products and (c) a single isolated nanofiber observed after dispersion at very low concentration. Image magnification is 4500× in b and 5000× in c. (d) Tapping mode atomic force microscopy topographic image of a single organic nanofiber on a gold film. (e) Height profile taken along the dotted line in d. Fiber height is measured to be about 300 nm and its apparent width is about 450 nm due to tip-sample convolution.

Photoluminescence of a single nanofiber on glass

Far-field optical excitation is used to characterize the photonic guided modes of a single nanofiber on *glass*. Characterization of the native guided modes of the organic nanofibers *without the gold film* is necessary so that the mixed photonic-plasmonic character of the guided modes in the hybrid nanofiber-on-gold system may be evident. Figure 2 shows optical Fourier space images of the emitted light obtained with different bandpass filters before the detector. Such data reveals the spectral dependence of the angular emission pattern in the glass substrate. The in-plane orientation of the nanofiber is shown in Figs. 2a and g. Remarkably, two emission contributions may be readily distinguished in Fourier space. First of all, an emission ring appears at a radial coordinate that corresponds to the critical angle for an air|glass interface ($\theta_c \approx 41°$), independent of the emission wavelength. This almost azimuthally isotropic contribution resembles the radiation pattern of a point-like electric dipole on an air|glass interface;[24] therefore, we ascribe it to the direct emission of the molecules into the substrate. Secondly, an anisotropic component of the emission, directed along the nanofiber axis, appears to have its maximum at a radial coordinate that exceeds the accessible area of Fourier space. We attribute this contribution to molecular emission into a guided mode of the nanofiber. The refractive index of the bulk organic material composing the nanofiber[25] is given to be $n = 1.631$, which is higher than that of the glass substrate ($n = 1.518$), thus enabling waveguiding in the nanofiber without out-coupling into light in the substrate. Nevertheless, the dispersion curve of the guided mode has a finite width due to losses and we detect some light at the edges of the accessible angular domain (corresponding to $n = 1.45$). Interestingly, the relative intensity of this contribution in the Fourier image increases with the detection wavelength λ_0. This may be due to an increase in the losses, or because the effective index of the guided mode decreases, due to both the chromatic dispersion of the material and the geometric confinement of the waves in the nanofiber.

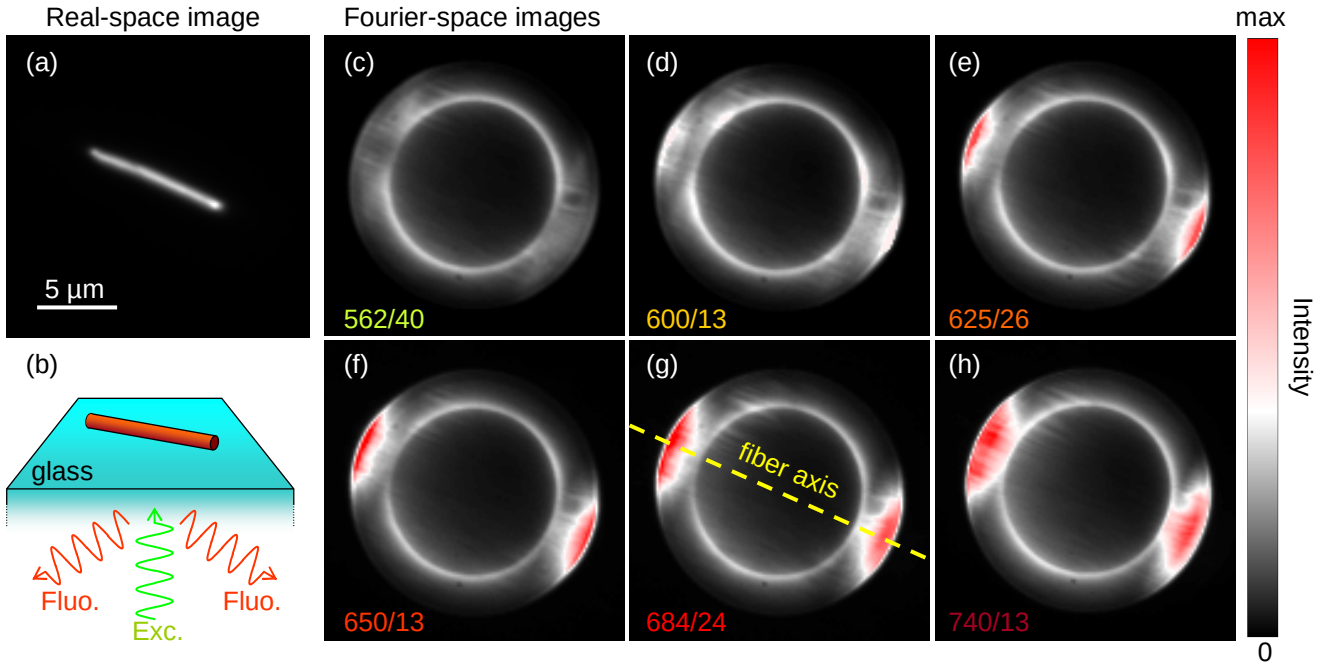

Figure 2: Fluorescence of a single organic nanofiber on glass upon optical excitation with a mercury-vapor (Hg) lamp (bandpass excitation filter at 488/10 nm). (a) Grey-scale fluorescence image in real space (longpass dichroic mirror starting at 525 nm). (b) Sketch of the excitation/emission geometry. (c-h) Fluorescence images in Fourier space in false color measured using different bandpass emission filters in addition to the longpass dichroic mirror: (c) 562/40 nm, (d) 600/13 nm, (e) 625/26 nm, (f) 650/13 nm, (g) 684/24 nm, (h) 740/13 nm. The dashed line in Fig. 2g indicates the axial orientation of the organic nanofiber. All fluorescence images are measured using an oil-immersion objective of numerical aperture NA = 1.45.

Photoluminescence of a single nanofiber on gold

We now focus on the photoluminescence properties of the hybrid system. Figure 3 shows a real-space fluorescence image of a single organic nanofiber on a thin gold film. One can see in this image both the direct light emission through the gold film (at the location of the nanofiber) and leakage radiation of the SPPs propagating away from the nanofiber (see supplementary information for more details). In order to determine the dispersion curves of the guided modes in the hybrid nanofiber-on-gold system, we analyze the photoluminescence of a single organic nanofiber on the thin gold film in Fourier space. We use the same excitation and detection conditions as for the Fourier-space images shown in Fig. 2. The Fourier images shown in Fig. 3 have two recognizable features. First of all, a narrow ring appears at the expected wavenumber for SPPs propagating at an air|gold interface; hence this corresponds to the leakage radiation of SPPs launched on the gold film. Secondly, straight narrow lines located orthogonally to the nanofiber axis are seen. Such lines in Fourier space denote the presence of waves propagating along a quasi-1D waveguide;[26] thus they may to be ascribed to guided modes of the nanofiber-on-gold-film system. Interestingly, the signature of the guided modes in Fig. 3c-h strongly differs from that seen in Fig. 2c-h where the organic nanofiber is on glass. In particular, the guided modes in the organic nanofiber on the gold film have lower effective indices (the lines are closer to the Fourier space origin), and the lines appear narrower, suggesting that the losses are lower. The lower effective indices support the idea that these are mixed photonic-plasmonic guided modes. Interestingly, some of the Fourier images (Fig. 3c,d) exhibit *two* parallel straight lines on each side of the narrow ring, due to coexistence of *two* guided modes.

Figure 4a shows the effective indices of the two guided modes as determined from Fig. 3c-h and plotted as a function of emission wavelength. The resulting dispersion relations may be represented in the usual energy-*vs*-wavevector plot as shown in Fig. 4b. As well, an effective index is associated with SPP propagation on the gold film, which is deduced from the radius of the narrow ring in Fig. 3c-h. As expected, good agreement with the theoretical dispersion

curve of SPPs propagating at an air|gold interface is found.[27,28] It appears readily in Fig. 4b that an existence condition for guided modes in the hybrid system is that the effective index must be higher than that of SPPs at an air|gold interface.

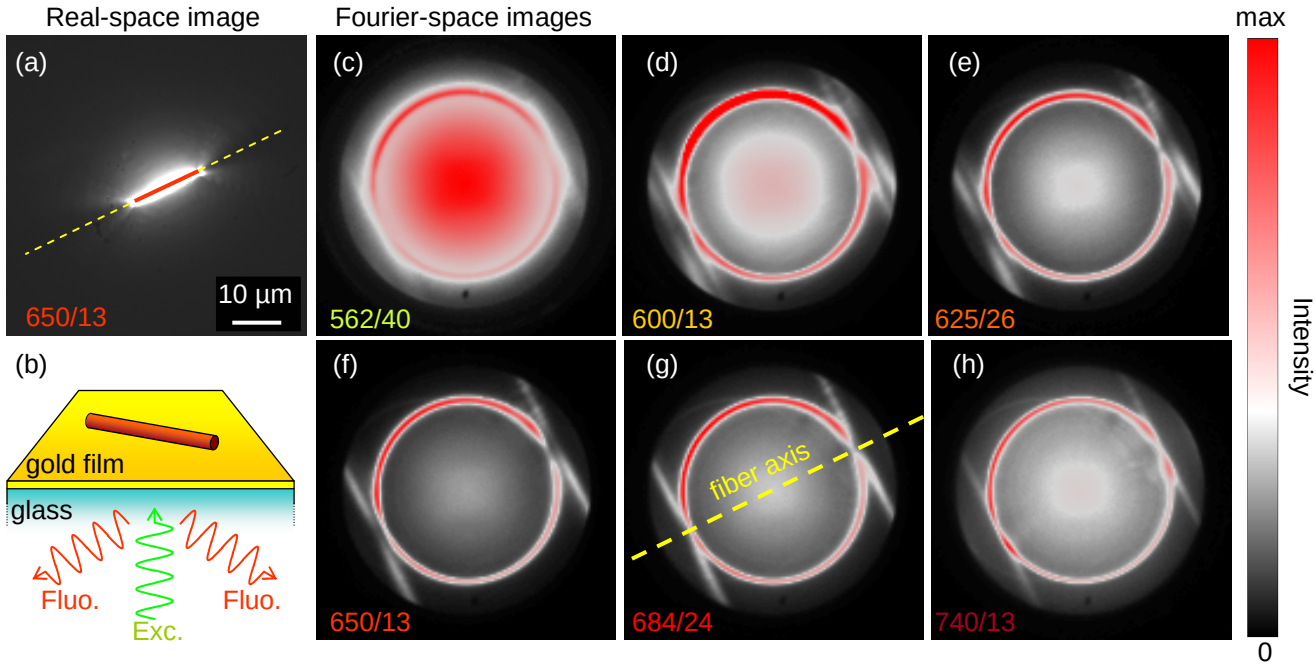

Figure 3: Fluorescence of a single organic nanofiber on a thin gold film (50 nm) upon optical excitation with a Hg lamp (same conditions as in Fig. 2). (a) Grey-scale fluorescence image in real space (bandpass emission filter: 650/13 nm). (b) Sketch of the excitation/emission geometry. (c-h) Fluorescence images in Fourier space in false color, measured using different bandpass emission filters: (c) 562/40 nm, (d) 600/13 nm, (e) 625/26 nm, (f) 650/13 nm, (g) 684/24 nm, (h) 740/13 nm. The dashed yellow line in Fig. 3g indicates the axial orientation of the organic nanofiber.

In order to further identify the guided modes, we examine the theoretical electric field distribution in and nearby an organic nanofiber on a gold film. Numerical FDTD calculations are performed using the free software MEEP.[29] The luminescence of the molecules in the fiber is simulated by considering a point-like, monochromatic, electric dipole in the center of a dielectric cylinder and the energy density of the electric field is monitored in a vertical cross-section far (≥ 2 μm horizontally) from the dipole. Figure 5 shows the results obtained for two different emission wavelengths, each of which exhibits a distinct electric field pattern. At the lower energy ($\mathcal{E} = 1.77$ eV, i.e., $\lambda_0 = 700$ nm), a single guided mode is excited in

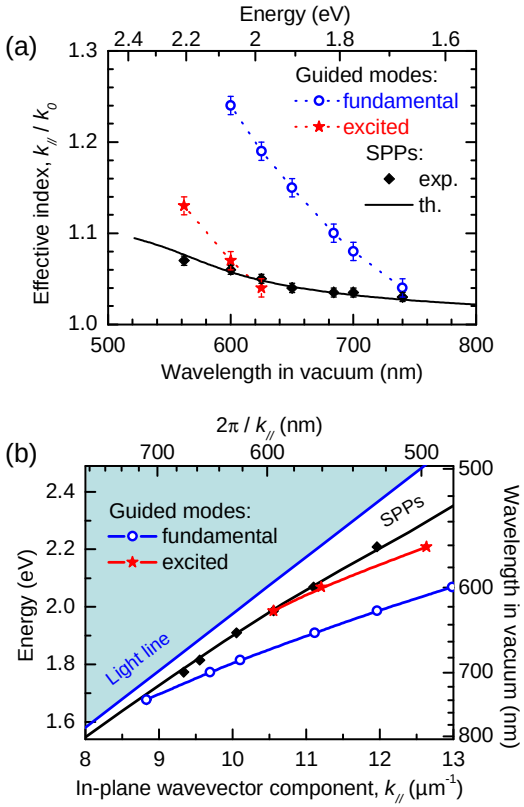

Figure 4: Dispersion relations for the guided modes of the organic nanofiber/gold film system. (a) Effective refractive index of SPPs and guided modes *versus* the emission wavelength in vacuum λ_0. The SPP effective refractive index is determined from the radius of the light ring in the Fourier-space images shown in Fig. 3; for the guided modes the Fourier coordinate (along the nanofiber axis) of the straight lines in Figs. 3c-h is used. The theoretical effective index of SPPs (k_{SPP}/k_0 with $k_0 = 2\pi/\lambda_0$) is also shown. (b) Plot of the energy $\mathcal{E}$ *versus* the in-plane wavevector component $k_{\|}$ of the SPPs and the guided modes in the organic nanofiber/gold film system. The light line corresponds to $\mathcal{E} = \hbar c k_{\|}$ and the shaded area is the light cone, representing all the possible plane waves in air.

the nanofiber, and the electric field is mainly concentrated at the fiber/gold film contact line (see Fig. 5b). The electric field is mainly orthogonal to both the gold film and the nanofiber axis and its direction is constant within the section of the fiber. We therefore describe this "fundamental" guided mode as a combination of the plasmonic (SPP) mode of the air|gold interface and the linearly polarized photonic mode LP01 of the nanofiber.[30] At higher energy ($\mathcal{E}$ = 2.07 eV, i.e., λ_0 = 600 nm), two modes are observed. One mode is similar to the fundamental mode occurring at lower energy, while the other exhibits two local maxima of electric field density, namely at contact with the film and atop the fiber. In the latter mode, a node occurs at the center of the fiber and the electric field changes direction when crossing this node (see Fig. S4 in the supplementary information for more details). Hence we refer to this "excited" guided mode as a combination of the SPP mode of the air|gold interface and the LP11 photonic mode of the nanofiber.

Coupling an electrical SPP nanosource to a nanofiber on gold

We now address the coupling of a local, *electrical* SPP nanosource to the hybrid system *optically* characterized above. As illustrated in Fig. 6a, we launch circular SPP waves on the gold film from the tip of an STM[23,32–34] (SPPs are excited by inelastic electron tunneling) and we monitor the coupling of these waves into the guided modes of the nanofiber-on-gold system. For this study, we use both real and Fourier-space leakage radiation microscopy and we study the effect of the tip excitation position on the emitted radiation. Figure 6 shows the dependence of the coupling efficiency on the transverse position of the tip with respect to the nanofiber axis (Fig. 6f summarizes the investigated configurations). When the tip is on-axis (Fig. 6b), the nanofiber appears bright and clearly stands out compared to the leakage radiation background in the real-space image; in other words, coupling is highly efficient. Conversely, the nanofiber looks relatively dark (yet with bright side edges) for off-axis tip positions (Fig. 6c-e), suggesting low coupling efficiency. Hence we infer that the coupling efficiency of the SPP waves to the guided modes of the nanofiber/gold film system depends

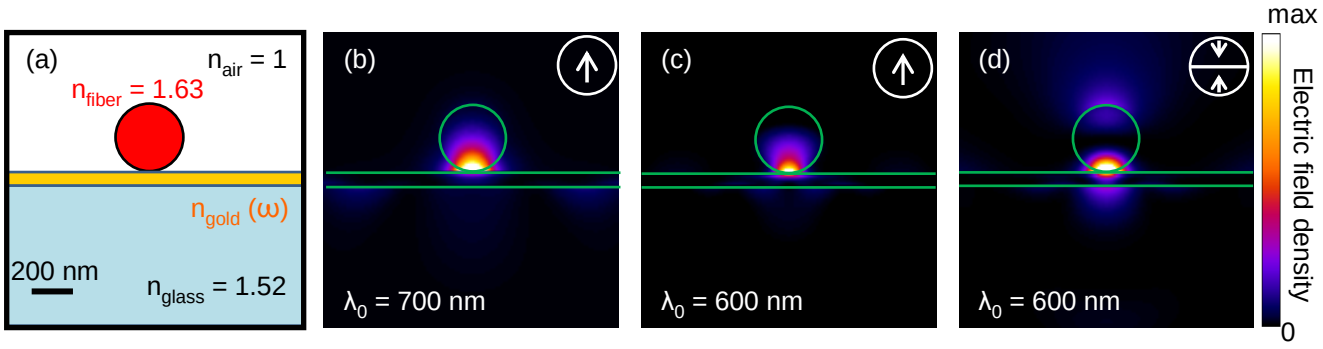

Figure 5: Identification of the guided modes in the organic-nanofiber-on-gold-film system, as derived from finite-difference time-domain (FDTD) calculations. (a) Schema of a vertical cross-section of the 3D calculation box indicating the refractive indices used in the model. Dielectric constants of gold are obtained from a Drude-Lorentz theory.[31] In these numerical simulations, we consider a point-like, monochromatic, electric dipole in the center of the cylindrical fiber and we examine the energy density of the electric field ($\frac{1}{2}\epsilon|E|^2$) in a vertical cross-section located about 2 μm from the dipole. (b-d) Results of the FDTD calculations for energies $\mathcal{E}$ = 1.77 eV (i.e., λ_0 = 700 nm) and $\mathcal{E}$ = 2.07 eV (i.e., λ_0 = 600 nm). A guided (fundamental) mode resembling an LP01 mode is observed at the lower energy (b), whereas two guided modes, resembling a (fundamental) LP01 mode and an (excited) LP11 mode occur at higher energy (c,d). As both modes are excited at this higher energy, a distinct field distribution pattern cannot be separately obtained for each mode; however, an approximation is found by examining two vertical cross-sections at two different distances from the dipole, corresponding to density minima of (c) the "LP11" mode and (d) the "LP01" mode, respectively. All FDTD calculations are performed using the free software MEEP.[29]

critically on the incidence angle. Optimal coupling efficiency exists for SPPs propagating parallel to the nanofiber axis.

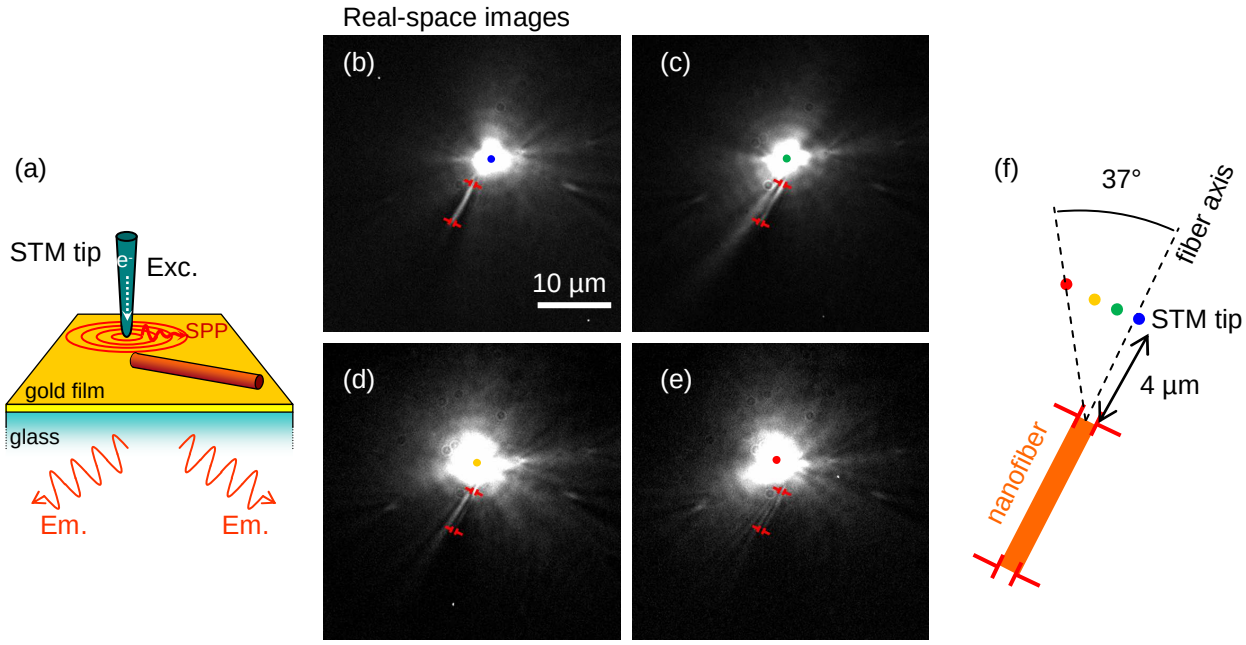

Figure 6: In-coupling of electrically excited SPPs into the guided modes of the organic-nanofiber-on-gold-film system: coupling efficiency. (a) Sketch of the excitation/emission geometry: the STM current generates a local, broadband in energy, nanoscale source of circular SPP waves that propagate on the gold film away from the tunnel junction and interact with the nanofiber. (b-e) Grey-scale real-space optical images, measured using the full spectrum (typically centered at $\lambda_0 \approx 700$ nm and about 150 nm-wide at half maximum),[32] with the STM tip located at four different sites on the gold film (indicated by colored dots as shown in f), i.e., (b) the tip is along the fiber axis, 4 μm away from the fiber end, or (c-e) off-axis by (c) 1 μm, (d) 2 μm or (e) 3 μm. The sample is biased to 2.5 V and the tunnel current setpoint is 1 nA. Optical image acquisition time is 300 s. The T-shaped markers indicate the ends of the organic nanofiber (length 6.2 μm).

Next we measure the light emitted from the nanofiber in Fourier space in order to confirm that SPPs couple into guided modes and to compare these modes with the guided modes uncovered in our optical photoluminescence study. For this experiment, we use a slightly modified setup as detailed in Fig. 7. A pinhole is set in the image plane in order to select the light emitted from an area including the nanofiber but excluding the tip location. This spatial filtering is necessary so that the intense direct light emission from the tip is excluded, so that any weaker contribution from the nanofiber may be observed (the observations made

in Fourier space in absence of spatial filtering are discussed below in Figs. 8 and 9). In this way, we measure the angular distribution of the light emitted from this specific area. An unavoidable drawback is that reducing the spatial area in real space degrades the angular resolution in Fourier space. The resulting Fourier image in Fig. 7c again exhibits two recognizable features. An arc slightly above the critical angle and corresponding to SPP leakage radiation is identified; this feature is not a full circle since the spatial filtering limits the direction of the collected emission. Also, a straight line appears at higher angles, orthogonal to the nanofiber axis. Such a line is again the signature of a guided mode.[26] This suggests that the emitted light seen along the nanofiber in the real-space image (in Fig. 6b) may be attributed to a guided mode, thus ruling out other eventualities, e.g., SPP scattering at the nanofiber edges. The effective index of the guided mode is measured from the location of the line in Fourier space to be 1.22 ± 0.05. This value only matches the index range of the "fundamental" guided mode discussed above. Hence we conclude that a local, electrical SPP nanosource may indeed couple energy into the guided modes of a hybrid system consisting of an organic nanofiber on a thin gold film, provided that the source is aligned along the nanofiber axis.

SPP-to-photon scattering at the nanofiber end

A central issue when coupling a local, electrical SPP nanosource to a hybrid system as described above is the coupling efficiency of the incident SPPs into the guided modes. SPP-to-photon scattering at the nanofiber end may result in significant losses. In this section, we study this scattering effect through the analysis of Fourier images recorded without spatial filtering. In contrast to the image shown in Fig. 7c, Fourier images without spatial filtering exhibit intense interference patterns. Figure 8 shows Fourier images recorded for different locations of the STM tip on the gold film along the axis of the nanofiber. The fringes do not occur at only one specific polar angle; rather they are visible within a polar range from the critical angle to the maximal collection angle. Hence we infer that the interference

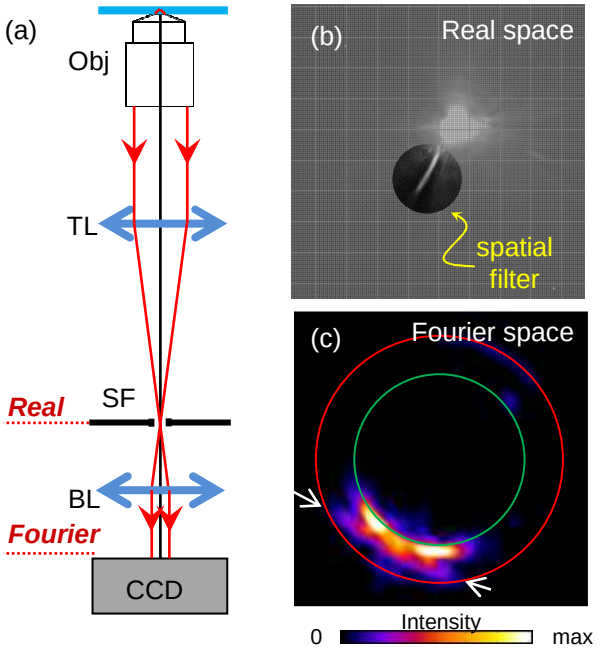

Figure 7: In-coupling of electrically excited SPPs into a guided mode of the organic-nanofiber-on-gold-film system: effective index. (a) Sketch of the experimental geometry used for spatially filtering the emission: a circular aperture is set in the image plane of the tube lens (TL) in order to select the light emitted within a 10-μm-diameter area centered on the nanofiber. The direct light emission from the tunnel junction is blocked, while the light emitted from the nanofiber is transmitted and imaged in Fourier space on the CCD camera using an extra lens (Bertrand lens, BL). (b) Same optical image in real space as Fig. 6b superimposed with a semi-transparent image of the aperture, illustrating the spatial filtering. (c) Corresponding optical image in Fourier space in false color, with the spatial filter set as shown in a and b. White arrows indicate the line corresponding to the guided mode in the nanofiber/gold film system. The sample is biased to 2.5 V and the tunnel current setpoint is 1 nA. Optical image acquisition time is 1800 s. The full emission spectrum is used as in Figs. 6b-e.

seen in Fig 8 is the result of the interaction of two light sources that have broad polar angular emission distributions in the substrate. This rules out leakage radiation of SPPs propagating on the gold film (narrow ring at $k_{\parallel} = k_{SPP}$) and guided modes propagating along the nanofiber (narrow lines at $k_{\parallel} = n_{eff}k_0$). Moreover, the fringe period $\Delta k_{\parallel}$ varies with the tip location following a $\frac{\Delta k_{\parallel}}{k_0} = \frac{\lambda_0}{d}$ variation where d is the distance between the tip and the proximal end of the nanofiber (see Fig. 9a). In other words, the tip and close end of the nanofiber behave as two coherent point-like light sources. This is so because both SPPs and light are emitted from the STM tip (see illustration in Fig. 9b). We have recently demonstrated the coherence of these two (light and SPP) emission channels.[35] The SPPs that are launched from the tip may scatter out of plane at the nanofiber into light in the substrate. This scattered light then interferes in the far field with the light directly emitted from the tip location. Below, we use this effect to retrieve information about the resulting phase shift of the emission from SPP-to-photon scattering at a nanofiber.

We note $\Delta\varphi(d,\theta)$ the total phase shift between the two coherent point sources mentioned above, i.e., the radiation under the tip and the SPPs scattered into light at the nanofiber (see Fig. 9b for the definitions of d and θ). $\Delta\varphi(d,\theta)$ includes the phase shift $\Delta\varphi_{path}(d,\theta)$ due to the optical path difference of the propagating waves as well as phase shifts $\Delta\varphi_{shift}(\theta)$ that may exist locally due to transmission through the gold film or upon SPP-to-photon scattering at the nanofiber end. From geometric considerations, we find that the first term reads $\Delta\varphi_{path}(d,\theta) = n_{glass}k_0 d\sin\theta - k_{SPP}d$. Therefore, the optical path difference is equal to zero for an emission angle corresponding to SPP leakage radiation (i.e., θ_{SPP}) in the tip-to-fiber direction. In absence of other phase shifts ($\Delta\varphi_{shift}(\theta_{SPP}) = 0$), a bright fringe tangent to the SPP leakage radiation light ring should be visible in the fringe pattern in Fourier space, regardless the value of d; yet, Fig. 9c shows that a dark fringe is observed instead. From this we infer that $\Delta\varphi_{shift}(\theta_{SPP}) \approx \pm\pi$. A more accurate estimation is possible by measuring the position of the two nearest bright fringes on both sides of the SPP leakage radiation. The results obtained for different tip-fiber distances are shown in Fig. 9d; thus

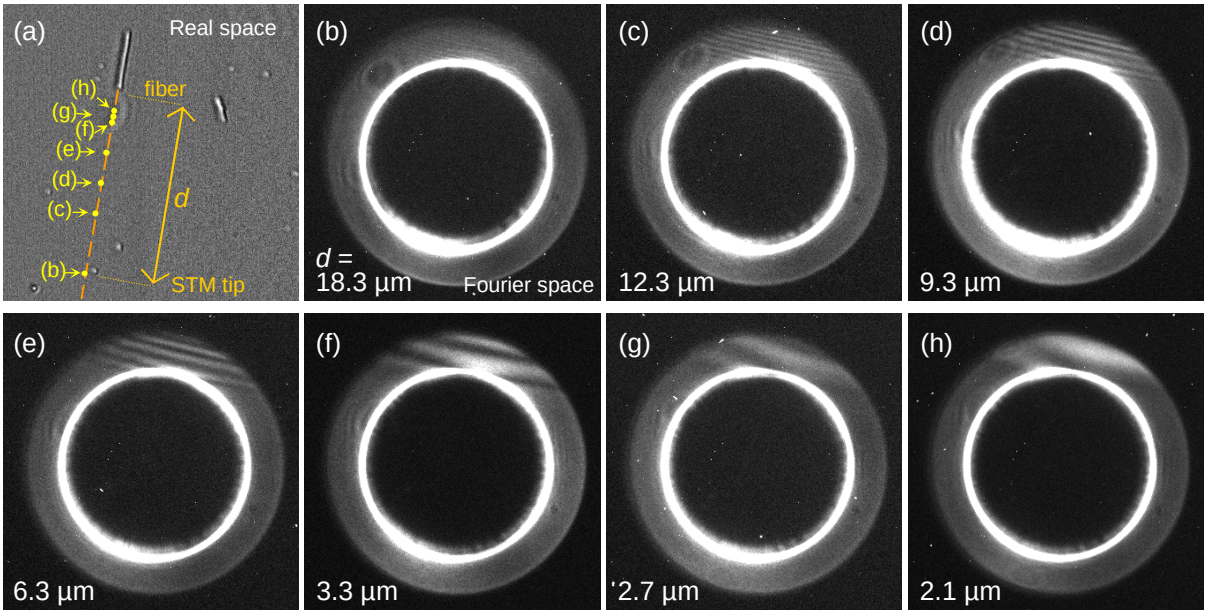

Figure 8: Scattering of electrically excited SPPs at an organic nanofiber on a gold film. (a) Transmission optical image of an organic nanofiber and the different tip excitation positions. (b-h) Grey-scale optical images in Fourier space, measured upon the electrical excitation of SPPs with the STM tip located along the fiber axis, at different distances d from the fiber end as indicated in (a), i.e. (b) $d = 18.3$ μm, (c) $d = 12.3$ μm, (d) $d = 9.3$ μm,(e) $d = 6.3$ μm, (f) $d = 3.3$ μm, (g) $d = 2.7$ μm and (h) $d = 2.1$ μm. The sample is biased to 2.5 V and the tunnel current setpoint is 1 nA. Optical image acquisition time is 300 s. The full emission spectrum is used as in Figs. 6b-e.

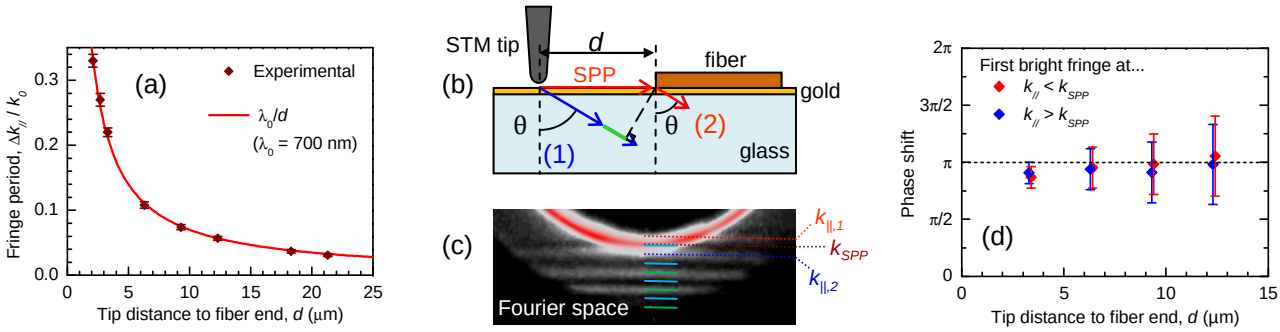

Figure 9: Scattering of electrically excited SPPs at an organic nanofiber on a gold film. (a) Fringe period of the interference patterns ($\frac{\Delta k_{\parallel}}{k_0}$) shown in Figs. 8b-h *versus* the in-plane distance d between the STM tip and the fiber end, as shown in Fig. 8a (points with error bars: experimental data; solid line: calculated values using a simple two-wave interference model, where $\frac{\Delta k_{\parallel}}{k_0} = \lambda_0/d$). (b) Sketch illustrating the two optical paths leading to interference in Fourier space (1: direct light emission from the tunnel junction; 2: SPP emission from the tunnel junction that propagates to and scatters into light at the fiber). (c) Detail of the Fourier image shown in Fig. 8e, showing the first bright fringes below ($k_{\parallel,1}$) and above ($k_{\parallel,2}$) the SPP leakage radiation (k_{SPP}) (see supplementary information for a vertical cross section of these fringes). (d) Phase shift $\Delta\varphi_{shift}$ evaluated from the relative position of the bright fringes at $k_{\parallel,1}$ and $k_{\parallel,2}$ in Fourier space *versus* the tip-fiber distance d. Within the investigated range of d ($[3, 13]$ μm), this phase shift is almost constant and equal to $(0.95 \pm 0.07)\pi$.

we estimate $\Delta\varphi_{shift}(\theta_{SPP}) = (0.95 \pm 0.07)\pi$.

Conclusion

We have investigated the combined photonic-plasmonic guided modes of an organic nanofiber on a gold film. In particular, we have shown that this hybrid nanostructure supports guided modes of lower index than the native modes of the nanofiber. A fundamental and an excited guided mode with different electric field density distributions coexist in this system. The dispersion relations have been determined from Fourier-plane photoluminescence measurements of the angular emission patterns at different energies.

As well, we have demonstrated that SPPs from a local, electrical STM-SPP nanosource may be coupled to such a hybrid system. The SPP waves from the STM tunnel current couple into the fundamental guided mode of the nanofiber/gold film system with maximal efficiency when the SPP propagation direction and nanofiber axis are collinear. An important part of the SPP energy, however, is scattered by the fiber out-of-plane into light. A phase shift of about π between this scattered light and the light emitted between the STM tip has been found.

These results highlight the processes that must be mastered so that the use of such hybrid photonic-plasmonic systems, e.g., for information transfer, will be efficient. For example, the ratio of SPPs coupled to the guided mode as compared to the SPPs scattered at the input end of the organic nanofiber must be improved. Such improvements may be achieved through optical impedance matching[36,37] by including plasmonic nanostructures (or optical nanoantennas) in the system.

Experimental

Organic nanofibers

The molecule diethyl 2,5-bis(phenylamino)terephthalate is synthesized according to the literature.[38] Nanofibers are grown via molecule recrystallization in nanoporous anodized aluminium oxide templates (Anodisc 13, Whatman Ltd.) according to a method described by Martin Steinhart *et al* for the growth of polymer nanofibers.[39] For this purpose the templates are cleaned in an ultrasonic bath with solvents of different polarity (water, acetone, toluene). A small amount of solid substance is deposited on the template and heated to 423 K under nitrogen atmosphere in a tube furnace. The produced fluid melt may then run into the nanopores. After cooling any residual material is removed from the template surface with a scalpel. The aluminum oxide template is dissolved in a 1.5 M sodium hydroxide solution for two hours. The as-obtained suspension of organic nanofibers is treated in an ultrasonic bath, filtered with a syringe filter (Durapore 0.22 μm PVDF membranes) and washed with water. From this procedure a powder of well-separated nanofibers is obtained. Scanning electron micrographs of the organic fibers shown in Fig 1b,c are recorded with a Hitachi S-3200N microscope.

Acknowledgement

This work was partly supported by the French RENATECH network. We acknowledge technical support from the "Centrale de Technologie Universitaire IEF-Minerve" in Orsay. We acknowledge the use of the computing facility cluster GMPCS of the LUMAT federation (FR LUMAT 2764). The authors (B.R., E.L.M., G.D. and E.B.D.) are grateful to H.-G. Rubahn and J. Fiutowski for fruitful discussions. We are also grateful to E. Jaskulska for assistance.

Supporting Information Available

Figure S1 shows a scanning electron micrograph of a nanoporous alumina matrix used for the synthesis of the organic nanofibers and histograms of the statistical diameter and length distribution of the fibers. As well, further results on the fluorescence of a single organic nanofiber on gold upon optical excitation are provided. In particular, these results verify that SPPs are launched from the nanofiber by the coupling of the nanofiber fluorescence into SPPs. As a complement to Fig. 3a, Figure S2 shows grey-scale fluorescence images in real space measured using different bandpass emission filters. Figure S3 shows a detailed analysis of these real-space images. As a complement to Fig. 5, we give in Figure S4 the theoretical distribution of the electric field components along x and z axis, which confirms the identification of the guided modes in the organic-nanofiber-on-gold-film system. Finally, intensity profiles taken from the Fourier images in Fig. 8 are plotted in Figure S5 to help the reader see the interference fringes.

This material is available free of charge via the Internet at `http://pubs.acs.org/`.

References

(1) Gramotnev, D. K.; Bozhevolnyi, S. I. Plasmonics beyond the diffraction limit. *Nat. Photon.* **2010**, *4*, 83–91.

(2) Sorger, V. J.; Oulton, R. F.; Ma, R.-M.; Zhang, X. Toward integrated plasmonic circuits. *MRS Bulletin* **2012**, *37*, 728–738.

(3) Massenot, S.; Grandidier, J.; Bouhelier, A.; Colas des Francs, G.; Markey, L.; Weeber, J.-C.; Dereux, A.; Renger, J.; Gonzàlez, M. U.; Quidant, R. Polymer-metal waveguides characterization by Fourier plane leakage radiation microscopy. *Appl. Phys. Lett.* **2007**, *91*, 243102.

(4) Oulton, R. F.; Sorger, V. J.; Genov, D. A.; Pile, D. F. P.; Zhang, X. A hybrid plasmonic

waveguide for subwavelength confinement and long-range propagation. *Nat. Photon.* **2008**, *2*, 496–500.

(5) Grandidier, J.; Massenot, S.; Colas des Francs, G.; Bouhelier, A.; Weeber, J.-C.; Markey, L.; Dereux, A.; Renger, J.; González, M.; Quidant, R. Dielectric-loaded surface plasmon polariton waveguides: Figures of merit and mode characterization by image and Fourier plane leakage microscopy. *Phys. Rev. B* **2008**, *78*, 245419.

(6) Holmgaard, T.; Chen, Z.; Bozhevolnyi, S. I.; Markey, L.; Dereux, A. Dielectric-loaded plasmonic waveguide-ring resonators. *Opt. Express* **2009**, *17*, 2968–2975.

(7) Reinhardt, C.; Seidel, A.; Evlyukhin, A. B.; Cheng, W.; Chichkov, B. N. Mode-selective excitation of laser-written dielectric-loaded surface plasmon polariton waveguides. *J. Opt. Soc. Am. B* **2009**, *26*, B55–B60.

(8) Grandidier, J.; Colas des Francs, G.; Massenot, S.; Bouhelier, A.; Markey, L.; Weeber, J.-C.; Finot, C.; Dereux, A. Gain-Assisted Propagation in a Plasmonic Waveguide at Telecom Wavelength. *Nano Lett.* **2009**, *9*, 2935–2939, PMID: 19719111.

(9) Grandidier, J.; Colas des Francs, G.; Massenot, S.; Bouhelier, A.; Markey, L.; Weeber, J.-C.; Dereux, A. Leakage radiation microscopy of surface plasmon coupled emission: investigation of gain-assisted propagation in an integrated plasmonic waveguide. *J. Microsc.* **2010**, *239*, 167–172.

(10) Schiek, M.; Balzer, F.; Al-Shamery, K.; Brewer, J. R.; Lützen, A.; Rubahn, H.-G. Organic Molecular Nanotechnology. *Small* **2008**, *4*, 176–181.

(11) Tavares, L.; Kjelstrup-Hansen, J.; Rubahn, H.-G. Efficient Roll-On Transfer Technique for Well-Aligned Organic Nanofibers. *Small* **2011**, *7*, 2460–2463.

(12) Bian, Y.; Gong, Q. Deep-subwavelength light routing in nanowire-loaded surface plas-

mon polariton waveguides: an alternative to the hybrid guiding scheme. *J. Phys. D: Appl. Phys.* **2013**, *46*, 445105.

(13) Balzer, F.; Bordo, V. G.; Simonsen, A. C.; Rubahn, H.-G. Optical waveguiding in individual nanometer-scale organic fibers. *Phys. Rev. B* **2003**, *67*, 115408.

(14) Schiek, M.; Balzer, F.; Al-Shamery, K.; Lützen, A.; Rubahn, H.-G. Light-emitting organic nanoaggregates from functionalized p-quaterphenylenes. *Soft Matter* **2008**, *4*, 277–285.

(15) Quochi, F.; Cordella, F.; Mura, A.; Bongiovanni, G.; Balzer, F.; Rubahn, H.-G. Gain amplification and lasing properties of individual organic nanofibers. *Appl. Phys. Lett.* **2006**, *88*, 041106.

(16) Kim, F. S.; Ren, G.; Jenekhe, S. A. One-Dimensional Nanostructures of π-Conjugated Molecular Systems: Assembly, Properties, and Applications from Photovoltaics, Sensors, and Nanophotonics to Nanoelectronics. *Chem. Mater.* **2011**, *23*, 682–732.

(17) Kjelstrup-Hansen, J.; Simbrunner, C.; Rubahn, H.-G. Organic surface-grown nanowires for functional devices. *Rep. Prog. Phys.* **2013**, *76*, 126502.

(18) Balzer, F.; Kankate, L.; Niehus, H.; Frese, R.; Maibohm, C.; Rubahn, H.-G. Tailoring the growth of p-6P nanofibres using ultrathin Au layers: an organic-metal-dielectric model system. *Nanotechnology* **2006**, *17*, 984.

(19) Radko, I. P.; Fiutowski, J.; Tavares, L.; Rubahn, H.-G.; Bozhevolnyi, S. I. Organic nanofiber-loaded surface plasmon-polariton waveguides. *Opt. Express* **2011**, *19*, 15155–15161.

(20) Skovsen, E.; Søndergaard, T.; Fiutowski, J.; Rubahn, H.-G.; Pedersen, K. Surface plasmon polariton generation by light scattering off aligned organic nanofibers. *J. Opt. Soc. Am. B* **2012**, *29*, 249–256.

(21) Leißner, T.; Lemke, C.; Fiutowski, J.; Radke, J. W.; Klick, A.; Tavares, L.; Kjelstrup-Hansen, J.; Rubahn, H.-G.; Bauer, M. Morphological Tuning of the Plasmon Dispersion Relation in Dielectric-Loaded Nanofiber Waveguides. *Phys. Rev. Lett.* **2013**, *111*, 046802.

(22) Huang, K. C. Y.; Seo, M.-K.; Sarmiento, T.; Huo, Y.; Harris, J. S.; Brongersma, M. L. Electrically driven subwavelength optical nanocircuits. *Nat. Photon.* **2014**, *8*, 244–249.

(23) Wang, T.; Boer-Duchemin, E.; Zhang, Y.; Comtet, G.; Dujardin, G. Excitation of propagating surface plasmons with a scanning tunnelling microscope. *Nanotechnology* **2011**, *22*, 175201.

(24) Lieb, M. A.; Zavislan, J. M.; Novotny, L. Single-molecule orientations determined by direct emission pattern imaging. *J. Opt. Soc. Am. B* **2004**, *21*, 1210–1215.

(25) `http://www.guidechem.com/dictionary/en/14297-59-7.html`.

(26) Hassan, K.; Bouhelier, A.; Bernardin, T.; Colas des Francs, G.; Weeber, J.-C.; Dereux, A.; Espiau de Lamaestre, R. Momentum-space spectroscopy for advanced analysis of dielectric-loaded surface plasmon polariton coupled and bent waveguides. *Phys. Rev. B* **2013**, *87*, 195428.

(27) Raether, H. *Surface Plasmons on Smooth and Rough Surfaces and on Gratings*; Springer Tracts in Modern Physcis; Springer-Verlag, Berlin, 1988; Vol. 111.

(28) Wang, T. Excitation électrique de plasmons de surface avec un microscope à effet tunnel. Ph.D. thesis, Université Paris-Sud, 2012.

(29) Oskooi, A. F.; Roundy, D.; Ibanescu, M.; Bermel, P.; Joannopoulos, J. D.; Johnson, S. G. Meep: A flexible free-software package for electromagnetic simulations by the FDTD method. *Comput. Phys. Commun.* **2010**, *181*, 687 – 702.

(30) Saleh, B.; Teich, M. *Fundamentals of Photonics*; John Wiley & Sons, 1991.

(31) Rakić, A. D.; Djurišić, A. B.; Elazar, J. M.; Majewski, M. L. Optical properties of metallic films for vertical-cavity optoelectronic devices. *Appl. Opt.* **1998**, *37*, 5271–5283.

(32) Wang, T.; Boer-Duchemin, E.; Comtet, G.; Le Moal, E.; Dujardin, G.; Drezet, A.; Huant, S. Plasmon scattering from holes: from single hole scattering to Young's experiment. *Nanotechnology* **2014**, *25*, 125202.

(33) Wang, T.; Comtet, G.; Le Moal, E.; Dujardin, G.; Drezet, A.; Huant, S.; Boer-Duchemin, E. Temporal coherence of propagating surface plasmons. *Opt. Lett.* **2014**, *39*, 6679–6682.

(34) Cao, S.; Le Moal, E.; Boer-Duchemin, E.; Dujardin, G.; Drezet, A.; Huant, S. Cylindrical vector beams of light from an electrically excited plasmonic lens. *Appl. Phys. Lett.* **2014**, *105*, 111103.

(35) Wang, T.; Rogez, B.; Comtet, G.; Le Moal, E.; Abidi, W.; Remita, H.; Dujardin, G.; Boer-Duchemin, E. Optical interferometry with a scanning tunneling microscope: a tool for studying surface plasmon polariton scattering by gold nanoparticles. *submitted*

(36) Greffet, J.-J.; Laroche, M.; Marquier, F. Impedance of a Nanoantenna and a Single Quantum Emitter. *Phys. Rev. Lett.* **2010**, *105*, 117701.

(37) Bigourdan, F. Plasmonic nanoantennas. Ph.D. thesis, Paris-Sud University, 2014.

(38) Zhang, Y.; Starynowicz, P.; Christoffers, J. Fluorescent Bis(oligophenylylamino)terephthalates. *Eur. J. Org. Chem.* **2008**, 3488–3495.

(39) Steinhart, M.; Wehrspohn, R. B.; Gösele, U.; Wendorff, J. H. Nanotubes by Template Wetting: A Modular Assembly System. *Angew. Chem. Int. Ed.* **2004**, *43*, 1334–1344.

Graphical TOC Entry